

Received July 30, 2020, accepted August 25, 2020, date of publication September 7, 2020, date of current version September 22, 2020.

Digital Object Identifier 10.1109/ACCESS.2020.3022171

Theoretical Analysis of Parameter Optimization for Lower-Ionosphere Excitation ELF/VLF Waves Based on Chirp-BOK Modulated Heating

KAIJIE ZHOU^{1,2}, HUALI WANG², (Member, IEEE), AND PEIPEI CAO^{1,3} 

¹College of Physics and Electrical Engineering, Huaiyin Normal University, Huai'an 223300, China

²Institute of Communications Engineering, PLA Army Engineering University, Nanjing 210007, China

³School of Electronic and Optical Engineering, Nanjing University of Science and Technology, Nanjing 210094, China

Corresponding author: Huali Wang (huali.wang@ieee.org)

This work was supported by the National Natural Science Foundation of China under Grant 61271354.

ABSTRACT To improve the anti-interference for ELF/VLF communication based on modulated heating lower-ionosphere, chirp spread spectrum technology with strong anti-interference is combined with square wave amplitude modulation, a novel method of chirp-BOK modulated heating lower-ionosphere is proposed in this paper. On this basis, to improve the radiation efficiency of ELF/VLF, the effects of heating parameters (effective radiation power, pump frequency, polarization mode, modulation frequency, duty cycle, and bandwidth) on the radiation efficiency of ELF/VLF were analyzed. The results show that the radiation amplitude of ELF/VLF increases with the increase of effective radiation power, while the radiation efficiency increases first and then decreases; the X-mode is better than the O-mode; the radiation intensity of ELF/VLF decreases with the increase of pump wave frequency from 4MHz to 10MHz; the ELF/VLF equivalent dipole moments increase with the rise of modulation frequency from 500Hz to 5kHz; with the change of duty cycle from 10% to 90%, the dipole moments first increase and then decrease, and the optimal range of duty cycle is 40% to 70%; with the increase of bandwidth, the dipole moments are unchanged. Furthermore, the ELF/VLF dipole moments of square wave amplitude modulated heating ionosphere is unchanged before and after the chirp spread spectrum.


INDEX TERMS Chirp-BOK, ELF/VLF, ionosphere.

I. INTRODUCTION

Extremely low frequency (ELF:0.3-3kHz) and very low frequency(VLF:3-30kHz) radio wave has very efficient long-range propagation in the earth-ionosphere waveguide and relatively deep penetration into conducting media, such as earth and seawater. Consequently, it has full applications ranging from naval communication to geophysical prospecting [1].

Since the wavelength of the ELF/VLF band is very long, direct radiation of the ground-based transmitter requires a large antenna, which is very difficult to achieve in engineering. In recent decades, ELF/VLF waves have been generated via modulated HF (high frequency) heating of the ionospheric D and low E regions [2]–[11]. The technology of ionospheric heating provided another possible ELF/VLF waves

generation mode. However, the low radiation efficiency of ELF/VLF is one of the key factors restricting its application in practical communication [7]. A lot of scholars are devoted to improving the radiation efficiency of ELF/VLF, and have proposed many original technologies and methods: beam scanning [9], geometric modulation [10], pre-heating amplitude modulation [12], Dual-beam heating [13], beat-wave method [14], etc. In [15], Cohen *et al.* presented a summary of nearly 100 days of ELF/VLF wave generation experiment at a variety of ELF/VLF frequencies, seasons, and times of day based on AM heating the ionosphere. They presented comprehensive statistics of generated ELF/VLF magnetic fields and several efficiency improvements had improved the ELF/VLF wave generation efficiency further. In 2010, they experimentally compared amplitude modulation, beam painting, and geometric modulation [16]. Their related researches have made remarkable progress. However, in the experiments of ionospheric heating, the design of

The associate editor coordinating the review of this manuscript and approving it for publication was Muhammad Zubair .

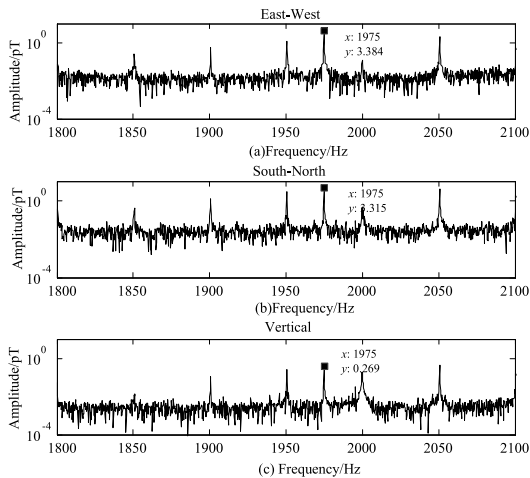


FIGURE 1. The amplitude spectrum of ELF signals received by SQUID.

complete communication schemes and the results of actual performance tests are rarely involved in the relevant articles. In [17], Jin *et al.* realized ELF/VLF communication rates of 100, 400, and 800bps by QPSK (quaternary phase shift keying). However, the ELF/VLF channel is always interfered with by strong power frequency harmonic, and the influence of harmonic interference on communication performance was not considered in [17]. In [1], under the influence of the load variation of generator and power grid, the power frequency harmonics still have a large range in the tens of harmonics. It was also pointed in the paper that the variation of fundamental frequency can be up to ± 0.1 Hz, so the variation at the 30th harmonic (i.e. 1.5kHz) can reach ± 3 Hz. In 2013, 100×100 m² square coils were used by the institute of microsystems of the Chinese academy of sciences to generate a single tone signal with a frequency of 1975Hz on the ground. They used the three-axis SQUID (Superconduction quantum interference device) to receive at 400m underground of a coal mine, and the measured amplitude spectrum is shown in Fig.1. As can be seen from Fig.1, ELF signals received in the three perpendicular directions all contained strong power frequency harmonic interference. To eliminate the influence of harmonics on ELF communication, the comb filter is always used to filter the harmonic interference in the broadband received signals, part of the signal components will be filtered at the same time. This will inevitably make the system BER(Bit error rate) performance deteriorated sharply.

The concept of spread spectrum(SS) was first proposed in the 1950s [18]. Because the spectrum of signals is broadened, the SS signals have strong anti-interference performance. According to different technical implementation, SS is usually divided into direct sequence, chirp modulation, frequency hopping and time-hopping [19]. Chirp modulation or linear frequency modulation was first proposed by Winkler in 1962 [20]. She suggested using a pair of linear chirps that have opposite chirp rates for binary signaling, which was generally called the chirp spread spectrum(CSS). CSS has the advantages of insensitivity to doppler frequency shift, resistance to narrow-band interference and impulse noise as well

as good robustness to power frequency harmonics [21], [22]. According to the role of the chirp signal in the modulation, the CSS is mainly classified into two categories, the direct modulation(DM) and binary orthogonal keying(BOK). The DM scheme uses the chirp signals as spreading code, and the data modulation and demodulation are performed separately from the chirp processing (e.g.chirp QPSK, chirp FSK). The chirp signals with positive and negative instantaneous frequency change rates in the BOK(Binary Orthogonal Keying) scheme are defined as up-chirp and down-chirp respectively. Because up-chirp and down-chirp have good auto-correlation and cross-correlation, they can be used to transmit bits '1' and '0' respectively. Therefore, to enhance the anti-interference performance and robustness of the ELF/VLF communication system, CSS is combined with the technology of modulation heating ionosphere in this paper. At present, the most commonly used modulation method in ionospheric heating experiments is amplitude modulation(AM), and the square wave AM has the highest radiation efficiency of ELF/VLF among the typical AM waves [13], [23].

Traditional ionospheric heating methods are all from the perspective of ionospheric heating. So a novel method of chirp-BOK modulated heating lower-ionosphere is proposed based on square wave AM from the perspective of communication in this paper. The combination of CSS and square wave AM(chirp-BOK) not only does not affect the radiation amplitude of ELF/VLF, but also increases the anti-interference ability of ELF/VLF communication. Furthermore, to improve the ELF/VLF radiation efficiency, we investigate heating parameters (effective radiation power, pump frequency, polarization mode, modulation frequency, duty cycle and bandwidth) on the radiation efficiency of ELF/VLF by chirp-BOK modulated heating lower-ionosphere at mid-low latitudes, and finally obtain many valuable conclusions, which may provide some constructive suggestions for choosing the best experimental parameters in ionospheric modulated heating experiments at mid-low latitudes in the future.

The remainder of this paper is organized as follows: In section 2, the ionospheric theoretical heating model based on square wave AM is introduced in detail. In section 3, the chirp-BOK modulation wave is designed in detail. In section 4, the proposed method of chirp-BOK is simulated and verified with the ionospheric heating model, and the ionospheric heating parameters of chirp-BOK is analysed in detail. The simulation results are discussed and summarized in section 5.

II. THE THEORETIC MODEL FOR MODULATED HF HEATING OF THE LOWER IONOSPHERE

The theory of current modulation is the basis of ELF/VLF generated by the HF wave periodic heating ionosphere. When a high power HF transmitter is turned on, the ionosphere begins to absorb the HF energy and increases in temperature. When the transmitter is turned off, the ionosphere cools to its ambient temperature and its conductivity returns to its ambient value. Thus, by varying the transmitter

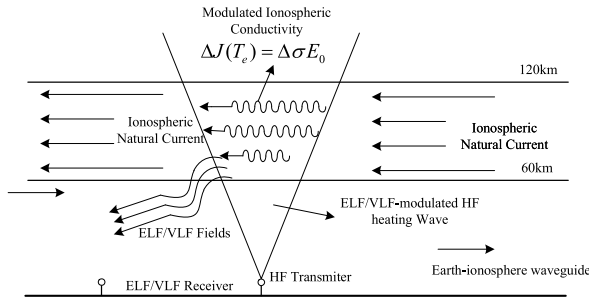


FIGURE 2. Cartoon depicting ELF/VLF waves generated via modulated ionospheric heating.

power at an ELF/VLF frequency, the ionospheric conductivity and currents vary at the same frequency to radiate the ELF/VLF waves. So the virtual antenna is formed in the lower ionosphere, as shown in Fig.2.

The electron temperature distribution is governed by the energy balance equation in the lower ionosphere during HF heating, neglecting the effects of electron thermal conductivity and plasma transport. The energy balance equation can be written as

$$\frac{3}{2}N_e k_B \frac{dT_e}{dt} = Q_{HF}(T_e, h) - L(T_e, h), \quad (1)$$

where N_e , T_e , k_B are the electron density, the heated electron temperature and the Boltzmanns constant respectively. $Q(T_e, h)$ is the absorption energy flow term for electron energy. $L(T_e, h)$ is the loss energy flow term for electron energy.

In the low ionosphere, the conductivity of the ionosphere σ is a function of electron density N_e and elastic collision frequency ν_{en} . The conductivity of the ionosphere σ is composed of Pedersen conductivity σ_P , parallel conductivity $\sigma_{//}$ and hall conductivity σ_H . The effect of parallel conductivity $\sigma_{//}$ is negligible at usual in the low ionosphere. The σ_H and σ_P can be expressed as

$$\sigma_H = \frac{N_e e}{B} \frac{\Omega_H^2}{\nu_{en}^2 + \Omega_H^2}, \quad (2)$$

$$\sigma_P = \frac{N_e e}{B} \frac{\Omega_H \nu_{en}}{\nu_{en}^2 + \Omega_H^2}, \quad (3)$$

where e and B are the electron charge and geomagnetic induction intensity respectively, $\Omega_H = 2\pi f_H$ is the cyclotron angular frequency. ν_{en} is the electron collision frequency which can be calculated from the empirical formula

$$\nu_{en} = 1.7 \times 10^{-11} [N_2] T_e + 3.8 \times 10^{-10} [O_2] T_e^{1/2} + 1.4 \times 10^{-10} [O] T_e^{1/2}, \quad (4)$$

where $[O]$, $[O_2]$, $[N_2]$ are the density of oxygen atoms, oxygen molecules and nitrogen molecules respectively.

In the time of the periodic modulation ionosphere, the period of ELF/VLF waves is very short. The period during which the electron density reaches a stable state is much longer than the modulation period, so the change of the electron density is not to be considered. The disturbances of the

ionospheric conductivity $\Delta\sigma$ (i.e. $\Delta\sigma_H$, $\Delta\sigma_P$) are generated by the HF waves periodic heating, and the formula is as follows

$$\Delta\sigma_H = -2 \frac{N_e e}{B} \frac{\nu_{en} \Omega_H^2}{\nu_{en}^2 + \Omega_H^2} \cdot \frac{d\nu_{en}}{dT_e} \cdot \Delta T_e, \quad (5)$$

$$\Delta\sigma_P = \frac{N_e e}{B} \frac{\Omega_H (\Omega_H^2 - \nu_{en}^2)}{\nu_{en}^2 + \Omega_H^2} \cdot \frac{d\nu_{en}}{dT_e} \cdot \Delta T_e. \quad (6)$$

The disturbances of the ionospheric conductivity can be expressed as $\Delta\sigma = \hat{x}\Delta\sigma_P + \hat{y}\Delta\sigma_H$. The electron electrojet current density under the the action of electric field E_0 is $\Delta J_s = \Delta\sigma \cdot E_0$.

The dipole moment M which is produced by heating the ionosphere can be expressed as:

$$M = \int_V \Delta J_s dV, \quad (7)$$

where V is the volume of disturbance region.

III. DESIGN OF ELF/VLF COMMUNICATION SCHEME BASED ON CHIRP-BOK

The simplest way to modulate the natural current is AM, which makes the HF carrier change with the amplitude of the signal. Its principle is the switch modulation, which is also the initial way to modulate the ionosphere. In [13], five common amplitude modulated waves were compared, and the results showed that the square wave AM was the most efficient one to generate ELF/VLF, and the triangular wave AM has the lowest efficiency. The ELF/VLF amplitude difference between the two modulation waveform is as high as 5dB. Therefore, the radiation efficiency of ELF/VLF can be effectively improved by designing appropriate modulation waveform. So, we choose to combine CSS with square waveform AM in this paper. First, the amplitude and power modulation functions of square wave AM are given as follows [11]

$$A_r(t) = D \sum_n P_{T/2}(t - \frac{T}{2} - nT_1) = D[1 + 2 \sum_{k=1} \text{sinc}(\frac{k\omega_1 T \pi}{2}) \text{cos}k\omega_1 t], \quad (8)$$

$$M_r(t) = A_r(t), \quad (9)$$

where D is duty cycle, $P_a(x) = 1$ for $|x| < a$ and 0 for $|x| > a$ is a square pulse function, T_1 is the period of modulation, $\omega_1 = 2\pi/T_1$.

Combining with CSS, the amplitude and power modulation functions of chirp-BOK can be expressed as

$$M_r(t) = A_r(t) = D[1 + 2 \sum_{k=1} \text{sinc}(\frac{k\omega_1 T \pi}{2}) \text{cos}k(\omega_1 t + \pi \mu t^2)], \quad (10)$$

where w_1 denotes the center frequency of the signal, μ denotes the rate of the linear frequency. The bandwidth of chirp signal is $B = |\mu|t$. When the symbol time T_1 is constant, the bandwidth increases with the increase of μ .

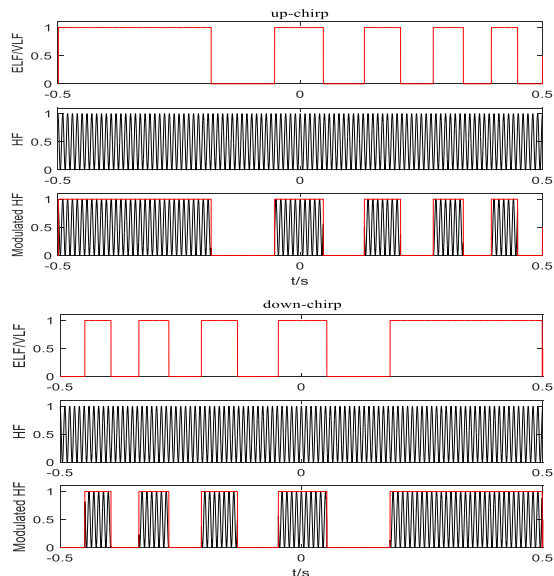


FIGURE 3. Time-domain waveform diagram of up-chirp and down-chirp.

As shown in Eq.(10), the signal of chirp is up-chirp for $\mu > 0$, and down-chirp for $\mu < 0$. Because up-chirp and down-chirp have a good feature of auto-relation and cross-correlation, up-chirp and down-chirp can be used to transmit information. The symbol '0' and '1' is represented by up-chirp and down-chirp respectively, which can be expressed as

$$\begin{cases} S_0(t) = D[1 + 2 \sum_{k=1} \text{sinc}(\frac{k\omega_1 T \pi}{2}) \cos k(\omega_1 t + \pi \mu t^2)] \\ -\frac{T_1}{2} < t < \frac{T_1}{2}, \\ S_1(t) = D[1 + 2 \sum_{k=1} \text{sinc}(\frac{k\omega_1 T \pi}{2}) \cos k(\omega_1 t - \pi \mu t^2)] \\ -\frac{T_1}{2} < t < \frac{T_1}{2}, \end{cases} \quad (11)$$

where $S_0(t)$ denotes up-chirp for transmitting symbol '0', and $S_1(t)$ denotes down-chirp for transmitting symbol '1'. For a more graphic understanding, the graphs of up-chirp and down-chirp with $T_1 = 1$ s, the data rate $R_b = 1/T_1 = 1$ bit/s, $\mu = 10$, $\omega_1 = 10\pi$, sampling rate $f_s = 1000$ are shown in Fig.3.

IV. NUMERICAL ANALYSIS AND DISCUSSION

In the numerical simulation, the parameters of neutral atmospheric background are calculated by MSISE90. The positive ions are only retained NO^+ and O_2^+ , and they are calculated by IRI-2016(International Reference Ionosphere 2016). As IRI-2016 model does not provide validated electron densities below 100km, the two-parameter model is more suitable [24]. Therefore, the electron densities are calculated using a two-parameter model below 100km, and above 100km, the electron densities are provided by the IRI2016 model. For the convenience of description, the model of the ionospheric electron densities used in this paper is referred to as T-IRI for short. The two-parameter model with h' in km and β in km^{-1}

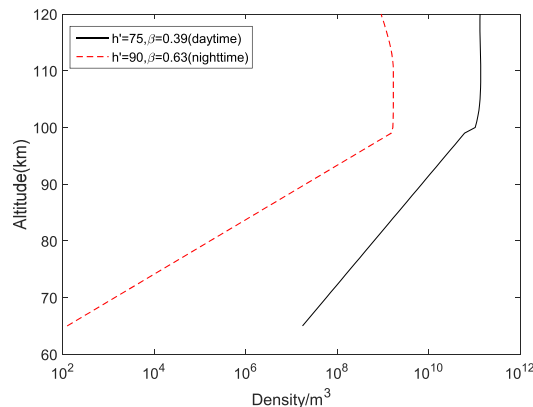


FIGURE 4. The ionospheric electron density profiles.

can be expressed by [25]

$$N_e(h) = 1.47 \times 10^{13} e^{-0.15h'} e^{(\beta-0.15)(h-h')} m^{-3}, \quad (12)$$

where $N_e(h)$ denotes the ionospheric electron density at the height of h km, the two-parameters h' and β denote a reference latitude and a gradient coefficient (steepness parameter) respectively. Nanjing, China ($31.14^\circ N$, $118.22^\circ E$) is selected as the geographical location of the research at 12:00 (noon) and 24:00 (midnight) BLT (Beijing time) on August 15, 2018. Because its geomagnetic latitude can be comparable to that at Arecibo ($28.28^\circ N$). So we choose $h' = 75$ km and $\beta = 0.39 \text{ km}^{-1}$ at daytime [26] and $h' = 90$ km and $\beta = 0.63 \text{ km}^{-1}$ at nighttime [27]. The ionospheric electron density profiles are shown in Fig.4.

In the selection of initial values of parameters, the initial values of electron temperature, ion temperature and neutral atmosphere temperature are equal to each other. The temporal resolution of the electronic temperature disturbance is $1 \mu\text{s}$, and the ionospheric height in the simulation ranges from 65 to 120 km with 1 km per layer. The disturbance of electron density is neglected because its time resolution is much larger than the period of heating ionosphere ($T_{heating} = 1/2f_{ELF/VLF}$). The background electric field E_0 is assumed to be 1 mV .

A. FEASIBILITY VERIFICATION OF CHIRP-BOK MODULATED HEATING LOWER-IONOSPHERE

First, we verified the feasibility of the chirp-BOK modulated heating lower-ionosphere. The simulation parameters are set as follows: the frequency of pump wave: 6 MHz, the effective radiation power (ERP): 200 MW, the polarization mode: O mode, duty cycle: 50%, the modulated waveform: chirp-BOK. As shown in Eq.(11), $T_1 = 0.01$ s, $\mu = 40000$, $\omega_1 = 2000\pi$, the center frequency of the signal $f_c = 1000$ Hz, the band of the signal $B = |\mu T_1| = 400$ Hz, the range of modulation frequency: 800 – 1200 Hz, sampling rate $f_s = 20000$, the communication rates: 100 bps.

When the ionosphere is heated by the chirp-BOK, the ionospheric electron temperature at 75 km varying with the heating time is shown in Fig.5. As can be seen from Fig.5, the frequency of electron temperature perturbation

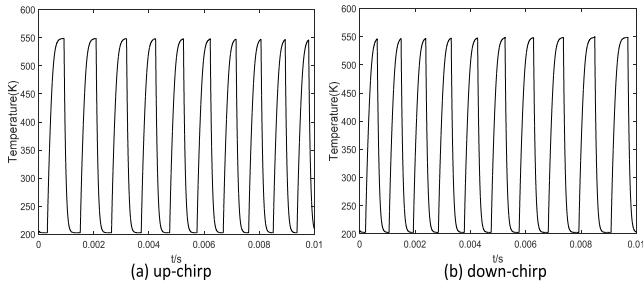


FIGURE 5. Electron temperature variations with time at 75km height.

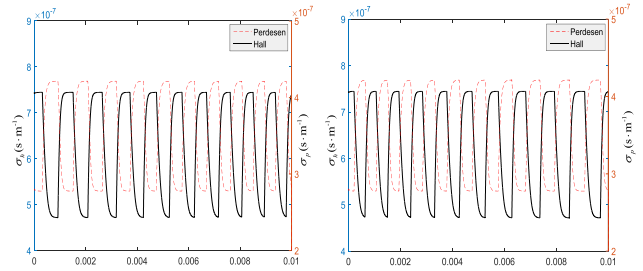


FIGURE 6. Pedersen and Hall conductivity variations with time at 75km height.

is changing. When up-chirp is used to heat the ionosphere, the disturbance frequency of the electron temperature increases from 800Hz to 1200Hz, which has the characteristic of up linear frequency modulation. When down-chirp is adopted, the frequency decreases from 1200Hz to 800Hz, which has the characteristic of down linear frequency modulation. Their center frequency is both 1000Hz so that '1' or '0' can be transmitted respectively. Visible from the figure, in the process of heating, electron temperature rapidly rises from 200K to 550K. In the process of cooling, the electronic temperature quickly decreases to the ionosphere background temperature. The periodic change of ionospheric conductivity caused by the repeated oscillation of ionospheric electron temperature is shown in Fig.6. The periodic change of conductivity leads to the periodic change of ionospheric current, as shown in Fig.7. Their perturbation period is consistent with the electron temperature, the central frequency is 1000Hz, and they all have obvious chirp characteristics. Eventually, a "virtual antenna" will be formed in the ionosphere to radiate ELF/VLF waves with chirp characteristics. In summary, the ELF/VLF radiation sources with chirp characteristics can be formed in the ionosphere by chirp-BOK, and thus ELF/VLF signals of up-chirp and down-chirp can be radiated to transmit information.

ELF/VLF waves with chirp characteristics can be excited effectively by the chirp-BOK heating ionosphere. When ELF/VLF is transmitted in the atmospheric channel, the anti-interference ability of ELF/VLF communication can be effectively improved. However, Will the combination of CSS and square wave AM affect the radiation amplitude of ELF/VLF? To compare the influence of square wave amplitude modulation on ELF/VLF radiation intensity before and after CSS, the simulation parameters are kept unchanged except that the

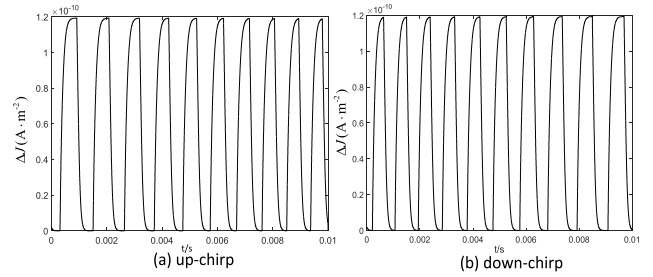


FIGURE 7. The current variations with time at 75km height.

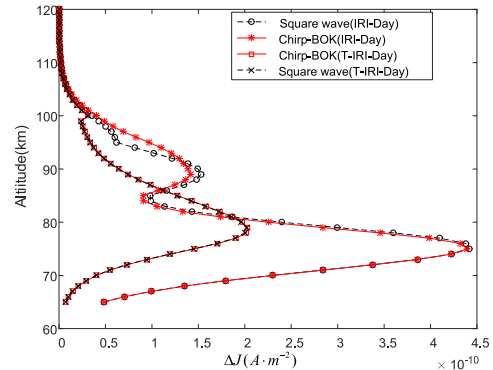


FIGURE 8. The profile of ionospheric current (Day).

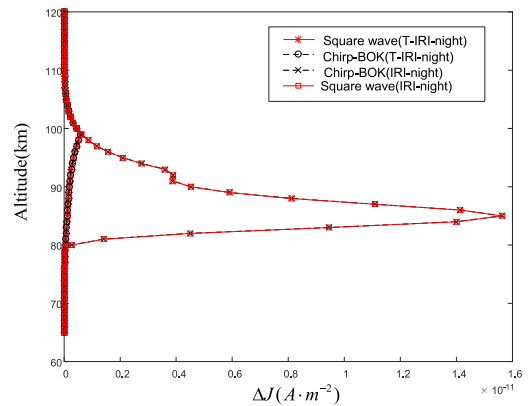


FIGURE 9. The profile of ionospheric current (Night).

frequency is changed to a fixed 1000Hz. The ionospheric current variation profiles of day and night are shown in Fig.8 and Fig.9 respectively.

As can be seen from Fig.8 and Fig.9, the current disturbance with IRI model is obviously larger than the T-IRI model both at daytime and nighttime, especially at nighttime. This is because the ionospheric electron density predicted by IRI model is higher than that of T-IRI model. Moreover, no matter which model is adopted, or whether it is at daytime or at night, the current disturbance does not change before and after CSS. This means that the amplitude of ELF/VLF excitation is also basically unchanged. Therefore, chirp-BOK heating ionosphere not only does not affect the radiation amplitude of ELF/VLF, but also increases the anti-interference ability of ELF/VLF communication. From the perspective of reception,

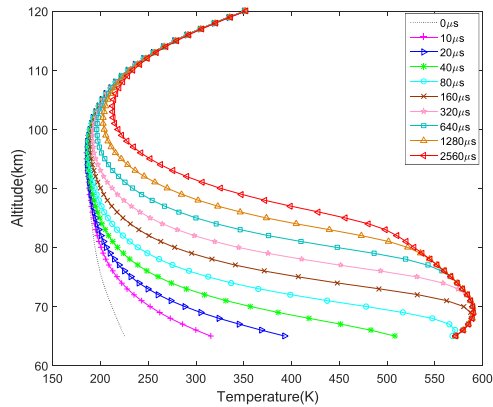


FIGURE 10. The profile of electron temperature heated by O mode.

it is equivalent to improving the radiation efficiency of ELF/VLF. As can be seen in Fig.8, the current disturbance with IRI model has visible bimodal peaks at about 75km and 90km respectively. The first peak is caused by the large amplitude of the electron temperature disturbance, while the other peak is caused by the sharp increase of the electron density at 85km-95km. However, the current disturbance with T-IRI model does not have similar characteristics. This is because the electron density below 100km is calculated by the two-parameter model, and the electron density does not increase significantly. As can be seen from Fig.9, the current disturbance at nighttime is significantly lower than that at daytime, because the ionospheric electron density is much higher at daytime than at nighttime. And the current disturbance with IRI model has not visible bimodal peaks, which is because IRI model does not provide the value of electron densities below 80km at night.

B. OPTIMIZATION ANALYSIS OF IONOSPHERIC HEATING PARAMETERS

To effectively improve the radiation efficiency of ELF/VLF, the chirp-BOK modulation heating the lower-ionosphere is simulated and analyzed from the parameters of polarization mode, ERP, the frequency of pump wave, modulation frequency, duty cycle and bandwidth.

1) POLARIZATION MODE

There are two polarization modes of HF electromagnetic wave heating ionosphere: X mode and O mode. The simulation parameters are set as follows: ERP:200MW, the frequency of pump wave:7MHz. For the convenience of comparison, the unmodulated continuous wave(CW) is used for heating. The background parameters are consistent with the above. The profile of the ionospheric electron temperature heated by O mode and X mode is shown in Fig.10 and Fig.11 respectively.

The CW is used to continuously heat the ionosphere from $0\mu s$ to $2560\mu s$, and the electron temperature at different heights tends to be saturated. As shown in Fig.8, when using O mode to heat the ionosphere, electron temperature appears a peak in about 70km, the highest temperature at about 580K.

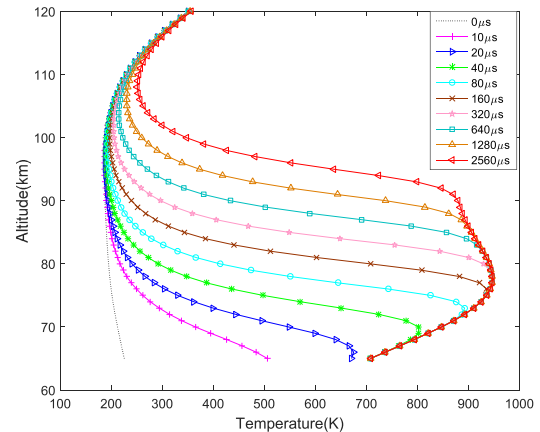


FIGURE 11. The profile of electron temperature heated by X mode.

From the perspective of view of time, when the heating time reaches $160\mu s$, the electron temperature at about 70 km no longer changes, and the temperature tends to be saturated. The electron temperature at other heights also tends to be saturated when the heating time reaches $2560\mu s$. When the ionosphere is heated by X mode, the profile of electron temperature at different heights is shown in Fig.11. When the heating time reaches $2560\mu s$, the electron temperature at different heights also tends to be saturated. There is a peak value of electron temperature at 75km in the ionosphere, and the maximum is about 950K. Compared to the O mode, the electron temperature disturbance amplitude of X mode is about 370K higher than that of O mode. Therefore, it can be seen from the simulation results that the X mode is more easily absorbed by the ionosphere than the O mode, and the X mode is more efficient than the O mode. In [28], Maxworth *et al.* observed in the experiment that ELF/VLF amplitude yielded by X mode was 3-10dB higher than O mode, that is, the X mode was more efficient than the O mode. And the conclusion obtained in this paper is consistent with this.

2) THE FREQUENCY OF PUMP WAVE

The simulation parameters are set as follows: ERP: 100MW, the frequency of pump wave is from 4MHz to 10MHz; the step size is 1MHz, the polarization mode: O mode. The ionosphere is continually heated by CW for 3ms, the profile of ionospheric electron temperature turbulence heated by different frequency of pump wave is shown in Fig.12. With the increase of pump wave frequency, the amplitude of electronic temperature disturbance gradually decreases. The amplitude of the electronic temperature disturbance is at the pump wave frequency of 4MHz, and the ionosphere height of about 70km is the largest, up to about 820K. In 2012, Cohen *et al.* experimentally compared the effect of HF frequency on ELF/VLF generation amplitude, and they found that generation in the Earth-ionosphere waveguide generally decreased with increasing HF frequency between 2.75-9.50 MHz [29]. And the conclusion obtained in this paper is consistent with this.

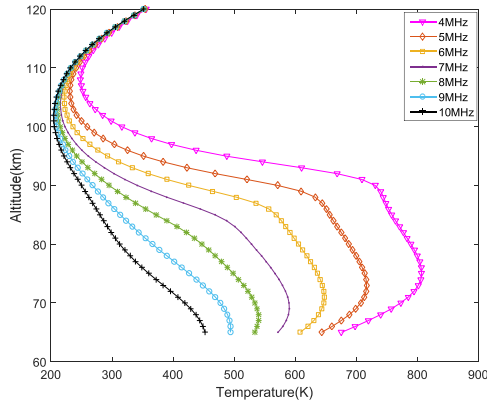


FIGURE 12. The profile of electron temperature with different frequency of pump wave heated by O mode.

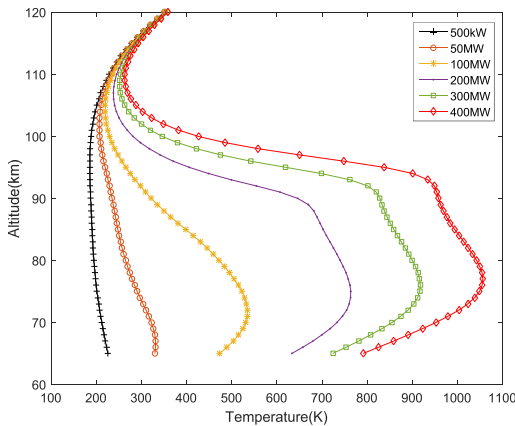


FIGURE 13. The profile of electron temperature with different ERP of pump wave heated by X mode.

3) ERP

The simulation parameters are set as follows: the frequency of pump wave: 7MHz, the polarization mode: X mode. The CW is used to continuously heat the ionosphere for 3ms, the profile of ionospheric electron temperature turbulence heated by X mode with different ERP is shown in Fig.13. With the increase of ERP, the amplitude of electronic temperature disturbance also increases. When ERP reaches 400MW, the electron temperature at about 75km can reach about 1100K, while when 500kW is used for heating, the electron temperature is only about 250K, the difference between the two is nearly 850K. Obviously, the higher the radiation intensity of ELF/VLF is when the ionosphere is heated by a more powerful pump wave. However, we find that when ERP increases from 500kW to 50MW, the temperature increase was very small, about 100K, when ERP increases from 50MW to 100MW, the temperature increases by about 200K, when the electron temperature increases from 100MW to 200MW, the electron temperature increases about 240K. When the power increases from 200MW to 300MW, the electron temperature increases by less than 140K. Similarly, the temperature increases by 100MW from 300MW are also less than 140K. Therefore, in terms of efficiency, ERP has higher ELF/VLF radiation efficiency at 100MW and 200MW.

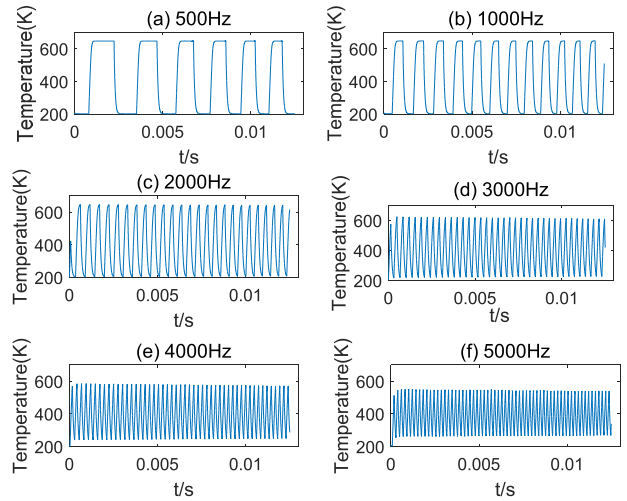


FIGURE 14. The electron temperature disturbance with different modulation frequencies(75km).

4) MODULATION FREQUENCY

The simulation parameters are set as follows: ERP:100MW, the frequency of pump wave: 7MHz, the polarization mode: X mode, duty cycle: 50%, the modulated waveform: chirp-BOK(up-chirp). As shown in Eq.(11), $T_1 = 0.0125s$, $\mu = 32000$, the band of the signal $B = |\mu T_1| = 400Hz$, sampling rate $f_s = 20000$, the communication rates: 80bps, $\omega_1 = 1000\pi, 2000\pi, 4000\pi, 8000\pi, 10000\pi$, that is, modulation central frequency $f_c = 500Hz, 1000Hz, 2000Hz, 3000Hz, 4000Hz, 5000Hz$. The turbulence of the ionospheric electron temperature at 75km with different modulation frequencies is shown in Fig.14.

When the center frequency $f_c = 500Hz, f_c = 1000Hz, f_c = 2000Hz$, the electron temperature can reach a maximum saturation temperature 650K in the heating period, and the cooling period, the electron temperature can also return to the background temperature. This is because the modulation frequency is low, the heating time T is larger than the heating time constant of ionospheric electron temperature τ_{heat} at 75km, the cooling time $T_1 - T$ is also larger than the cooling time constant of ionospheric electron temperature τ_{cool} . However, because the heating time T is too long, resulting in severe temperature saturation. This is particularly severe at the center frequency of 500Hz. With the increase of the modulation frequency, when the central frequency is 3000Hz, 4000Hz and 5000Hz, the electron temperature is not yet saturated in the heating period, and the electron temperature does not fall to the background temperature in the cooling period. This is because the heating time $T < \tau_{heat}$ and cooling time $T_1 - T < \tau_{cool}$, and this is more obvious when the central frequency is 5000Hz. The too low modulation frequency is easy to cause electron temperature saturation, which leads to a decrease of ELF/VLF radiation efficiency. The too-high modulation frequency is easy to cause small perturbation amplitude of the electron temperature, which leads to a decrease of ELF/VLF radiation amplitude.

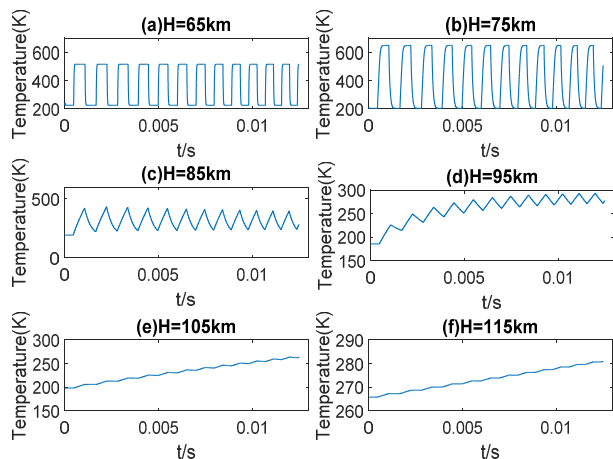


FIGURE 15. The electron temperature disturbance with different ionospheric heights.

So, when selecting the modulation frequency, the heating time T should be chosen to be close to τ_{heat} and the cooling time $T_1 - T$ to be close to τ_{cool} . Moreover, as the chirp-BOK modulation frequency is variable, the heating time T should be subject to the central frequency.

The heating and cooling time constant of ionospheric electron temperatures are different at different ionospheric heights. When the ionospheric height exceeds 95km, the time constant exceeds 15ms. If the modulation frequency is too large, it is difficult to cause the electronic temperature disturbance at this height. When the duty cycle is 50% and the center of modulation frequency is 1000Hz, the ionospheric electron temperature disturbance with different ionospheric heights is shown in Fig.15. As can be seen from Fig.15, the electron temperature cannot reach saturation at 85km in the heating period; the electron temperature is basically unchanged, especially at 105km. This is because the heating time T is far less than the heating time constant of ionospheric electron temperature at this height region. According to the previous analysis, different modulation frequencies correspond to different modulation period T_1 , and different ionospheric heights correspond to different time constants of electron temperature. Therefore, the influences of different modulation frequencies on electron temperature at different ionospheric heights are also different. However, the radiated ELF/VLF wave comes from the whole heating region, and its equivalent radiation source intensity, namely the dipole moment M , is obtained by the cumulative addition of the whole heating region. The dipole moment M with different modulation frequencies is shown in Fig.16.

It can be obviously seen from Fig.16 that the dipole moment M generated with the IRI model is larger than that generated with T-IRI model at daytime, and M generated with the T-IRI model at nighttime is 3-4 orders of magnitude smaller than that at daytime. This is because the ionospheric electron density predicted by IRI model is higher than that of T-IRI model, especially at nighttime. However, no matter which model is adopted, or whether it is in the daytime or at

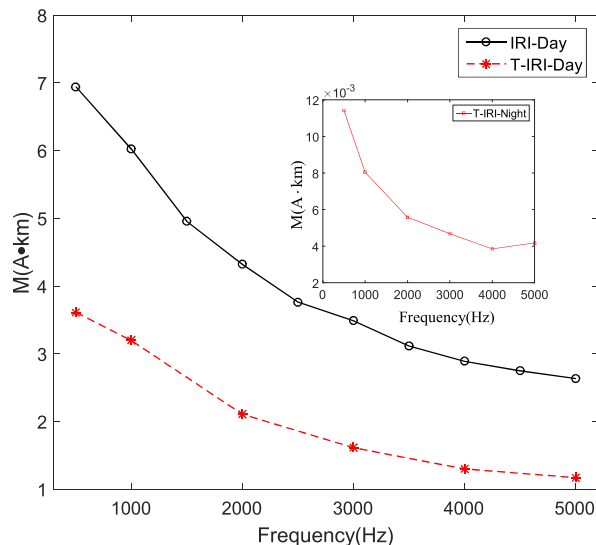


FIGURE 16. the dipole moment M with different modulation frequencies.

nighttime, all the dipole moment M decrease with the increase of the central modulation frequency. This is because the heating time decreases during the modulation period, the disturbance of the electron temperature decreases during the heating period and cooling period, resulting in the decrease of the disturbance amplitude of the electron temperature, which further leads to the decrease of M . Although M is decreasing with the increase of the modulation frequency, the trend of decline is more rapid when the modulation frequency is less than 2000Hz, and the trend is gradually slow down when the modulation frequency is greater than the 2000Hz. Furthermore, the lower-ionospheric ELF/VLF radiation source is around 75km. When the central modulation frequency is 2000Hz, the waveform quality is better than that of 500Hz. That is, there are fewer harmonic components in the ELF/VLF at the frequency of 2000Hz.

5) DUTY CYCLE

The simulation parameters are set as follows: ERP:100MW, the frequency of pump wave: 6MHz, the polarization mode: X mode, duty cycle: 50%, the modulated waveform: chirp-BOK(up-chirp). As shown in Eq.(11), $T_1 = 0.0125s$, $\mu = 32000$, the band of the signal $B = |\mu T_1| = 400Hz$, sampling rate $f_s = 20000$, the communication rates: 80bps, the modulation central frequency $f_c = 2000Hz$, the duty cycle: 10% ~ 90%, the step size is 10%. The electron temperature disturbance with different duty cycles is shown in Fig.17.

When the duty cycle is 10% ~ 40%, the electron temperature does not reach saturation in the heating period, but the electron temperature can fall back to the background temperature. When the duty cycle is 70% ~ 90%, the electron temperature can reach the saturation temperature of 650K, but cannot fall back to the background temperature of 200K from the maximum value of 650K. When the duty cycle is 70% ~ 90%, the electron temperature can not only reach the maximum 650K but also fall back to the ionospheric

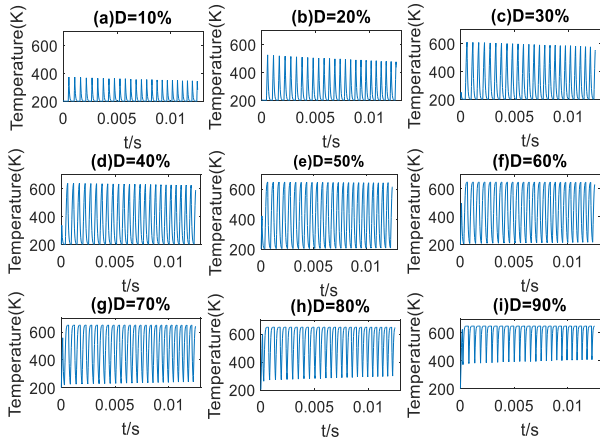


FIGURE 17. The electron temperature disturbance with different duty cycles(75km).

background temperature. This is because when the duty space is between 10% and 40%, the heating time constant of the electron temperature T is less than τ_{heat} at 75km, and the cooling time $T_1 - T$ is greater than τ_{cool} at 75km. As a result, the electron temperature cannot reach saturation in the heating period but can return to the background temperature in the cooling period. This is especially serious in the late heating period because the up-chirp gradually increases from 1800Hz to 2200Hz. The larger the modulation frequency, the smaller the heating time T , and the greater the difference with the heating time constant τ_{heat} , so the smaller the disturbance amplitude of electron temperature. As the duty cycle gradually increases to 40% ~ 70%, T increases and $T_1 - T$ decreases at the same time, satisfying $T > \tau_{heat}$ and $T_1 - T > \tau_{cool}$, the electron temperature can reach the maximum saturation value in the heating period, and the electron temperature can fall back to the background temperature in the cooling period. As the duty cycle gradually further increases to 80% ~ 90%, T further increases, and $T_1 - T$ further decreases at the same time. $T > \tau_{heat}$ and $T_1 - T < \tau_{cool}$ at this point, the electron temperature can be up to the saturation value, but cannot fall back to the background temperature. Although the maximum perturbation amplitude of the electron temperature can be obtained when the duty cycle is between 40% ~ 70%, the larger the duty cycle is, the greater the power consumption is. Therefore, it is more efficient when the duty cycle is 50%.

The dipole moment M with different duty cycles is shown in Fig.18. As can be seen from Fig.18(a), as the duty cycle increases, M generated with both IRI model and T-IRI model first increases and then decreases at daytime. This is because as the duty cycle increases, the heating time increases, and the increment of the electron temperature increases, leading to the increase of the disturbance amplitude of the electron temperature, and then M increases. As the duty cycle further increases, the cooling time decreases, and the drop of electron temperature decreases, leading to the reduction of the disturbance amplitude of the electron temperature, and then M decreases. Compared with the duty cycle of 10%,

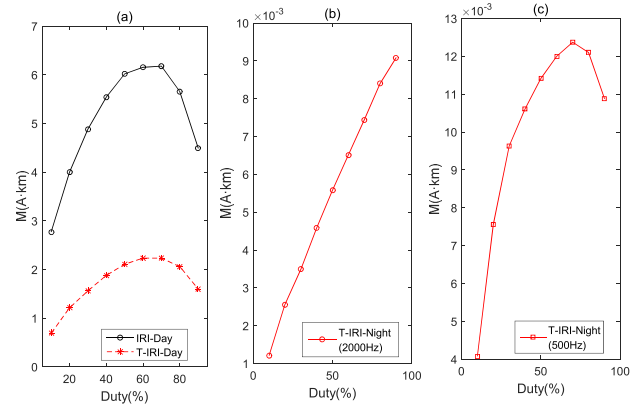


FIGURE 18. The dipole moment M with different duty cycles.

M is nearly two times higher when the duty cycle is 40% ~ 70%. Although M is the largest when the duty cycle is 70%, the electron temperature is saturated, and the waveform quality is poor. Therefore, from the perspective of ELF/VLF radiation efficiency, the duty cycle near 50% is the optimal choice. The dipole moment M with different duty cycles at nighttime are shown in Fig.18(b) and Fig.18(c). In Fig.18(b), the dipole moment M increases with the increase of duty cycle, which is different from the variation trend in Fig.18(a). This is because that the density of electrons at nighttime is mainly concentrated above 90km, and the heating time constant and the cooling time constant of the electron temperature at this height are relatively large, resulting in insufficient heating. As a result, the dipole moment M continues to increase with the increase of the duty cycle. When the modulation frequency is reduced from 2000Hz to 500Hz, as shown in Fig.18(c), the dipole moment M first increases and then decreases with the increase of duty cycle.

6) BANDWIDTH

The chirp-BOK signals have a certain bandwidth, and the frequency varies linearly within the band. The larger the time-bandwidth product BT of the chirp signal is, the stronger the anti-interference ability of the signal is. However, the value of BT cannot be infinite because of the transmission rate $R_b = 1/T$, the larger T , the smaller the transmission rate R_b . The bandwidth cannot be infinite too, especially the ELF/VLF band. To study the effect of bandwidth on ELF/VLF radiation efficiency, the simulation parameters are set as follows: ERP: 100MW, the frequency of pump wave: 6MHz, the polarization mode: X mode, duty cycle: 50%, the modulated waveform: chirp-BOK(up-chirp). As shown in Eq.(11), $T_1 = 0.0125s$, the communication rates: 80bps, the modulation central frequency $f_c = 2000Hz$, the duty cycle: 50%, sampling rate $f_s = 20000$, the band of the signal $B = |\mu T_1| = 100Hz, 400Hz, 800Hz, 1600Hz, 2000Hz, 3200Hz$. The electron temperature disturbance with different bandwidths is shown in Fig.19.

As can be seen from Fig.19, when the bandwidth B is less than 800Hz, the electron temperature can reach the maximum value without visible saturation in the heating period. It can

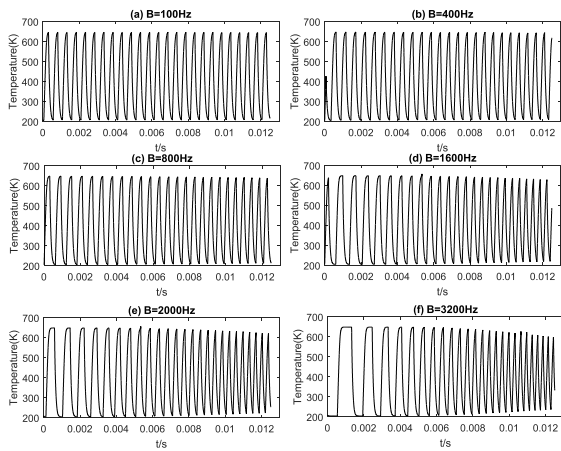


FIGURE 19. The electron temperature disturbance with different bandwidths(75km).

fall back to the background temperature in the cooling period. When the bandwidth B is larger than 1200Hz, the electron temperature gradually becomes saturated at the beginning of heating. In contrast, at the end of heating, the electron temperature increasingly fails to reach the maximum value, and it also fails to fall back to the background temperature at the end of cooling. This is because when the bandwidth is less than 800Hz, the frequency range is not extensive, and the heating time is close to τ_{heat} , so the initial stage of heating is not saturated, and the maximum value can be reached at the end of heating. When the bandwidth is higher than 1200Hz, especially at 3200Hz, the frequency reaches the lowest 400Hz and the highest 3600Hz. The frequency at the end of heating is too large, the heating time, the electron temperature cannot reach the maximum, and the cooling time, the electron temperature cannot fall back to the background temperature. At the beginning of heating, The frequency is too low, $T > \tau_{heat}$, the electron temperature is saturated. At the ending of heating, the frequency is too large, $T < \tau_{heat}$ and $T_1 - T < \tau_{cool}$, the electron temperature cannot reach the maximum value in the heating period and cannot fall back to the background temperature in the cooling period. The frequency-domain figures of the electron temperature disturbance with different bandwidths is shown in Fig.20. As can be seen from the figure, the spectral energy is all concentrated in the frequency band and distributed symmetrically at the central frequency of 2000Hz, in which the energy is mainly concentrated on both sides of the frequency band.

The dipole moment M with different bandwidths is shown in Fig.21. No matter which model is adopted, or whether it is at daytime or at nighttime, the dipole moment M is basically unchanged with the increase of bandwidth because the chirp-BOK signal is symmetric with the central frequency. Despite the rise of bandwidth, the signal is still symmetric on both sides, and the changes on both sides are opposite, which is precisely offset. Therefore, the dipole moment is basically independent of the bandwidth and related to the central frequency of the modulation. Besides, although increasing

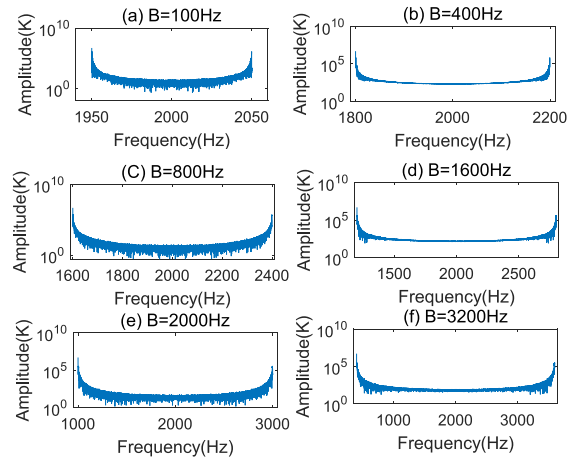


FIGURE 20. The frequency-domain figures of the electron temperature disturbance with different bandwidths(75km).

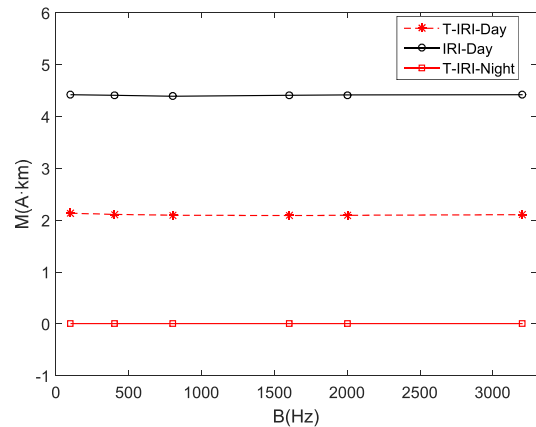


FIGURE 21. The dipole moment M with different bandwidths.

the bandwidth can increase the time-bandwidth product, to increase the anti-interference ability of the ELF/VLF communication, as the bandwidth increases, the signal quality also deteriorates. So, in the parameter selection, two aspects should be considered.

C. BER ANALYSIS OF CHIRP-BOK COMMUNICATION UNDER POWER FREQUENCY HARMONIC

As described above, the ELF/VLF band always interfered with by strong power frequency harmonics. In [1], under the influence of the load variation of generator and power grid, the power frequency harmonics still have an extensive range in the tens of harmonics. It was also pointed in the paper that the variation of fundamental frequency can be up to ± 0.1 Hz, so the variation at the 30th harmonic (i.e. 1.5kHz) can reach ± 3 Hz. To eliminate the harmonic interference, the comb filter is used to filter some signal components in the received signal, which makes the bit error rate(BER) of communication deteriorate rapidly. Therefore, numerical simulation of MSK, QPSK and chirp-BOK is carried out under a comb channel. In the simulation, a 3Hz comb filter is used to simulate the comb channel. The MSK, QPSK and chirp-BOK signal adopt non-differential modulation at the sending end and coherent

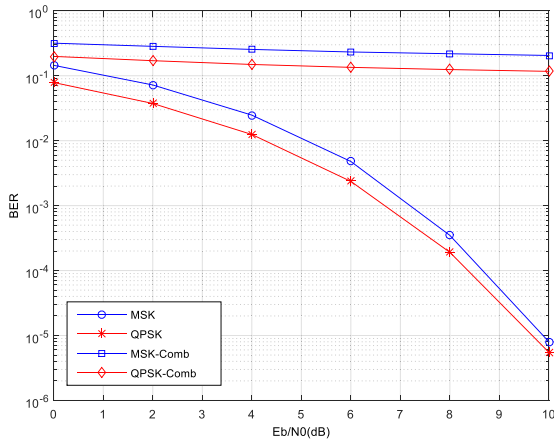


FIGURE 22. Performance comparison of QPSK and MSK before and after comb channel.

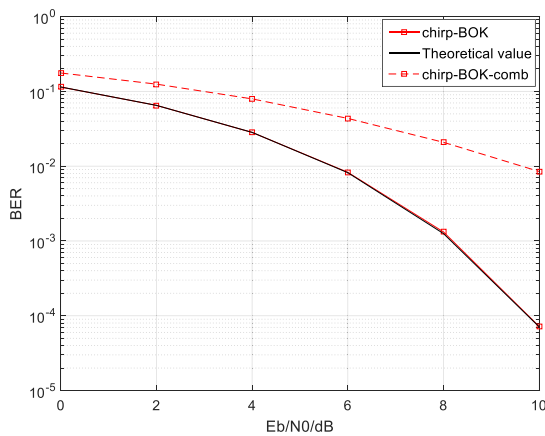


FIGURE 23. Performance comparison of chirp-BOK before and after comb channel.

demodulation at the receiving end. Performance comparison of QPSK and MSK before and after comb channel and Performance comparison of chirp-BOK before and after comb channel is shown in Fig.22 and Fig.23 respectively.

As can be seen from Fig.22, when the comb filter with a bandwidth of 3Hz is used to filter out harmonic interference, the performance of MSK and QPSK deteriorates seriously, which indicates that MSK and QPSK are all very sensitive to harmonic interference. The error performance of chirp-BOK with coherent demodulation is consistent with the theoretical value. And the BER of chirp-BOK also decreases to some extent after harmonic interference. However, the BER performance of chirp-BOK modulation is better than that of MSK and QPSK. This is due to the high time-bandwidth product, so it has a strong anti-interference ability and strong robustness of the system.

V. CONCLUSION

When the ionosphere is periodically heated by HF high-power waves, the ionospheric temperature and current will oscillate periodically to radiate ELF/VLF waves. Based on this, a novel method of chirp-BOK modulated heating lower-ionosphere is proposed in this paper to improve the

anti-interference for ELF/VLF communication. The two waveforms of up-chirp (symbol '0') and down-chirp (symbol '1') are respectively designed and verified by using ionospheric heating model. Furthermore, to improve the radiation efficiency of ELF/VLF, the effects of heating parameters (effective radiation power, pump frequency, polarization mode, modulation frequency, duty cycle, and bandwidth) on the radiation efficiency of ELF/VLF were analyzed. The relevant conclusions are summarized as follows:

- (1) the radiation amplitude of ELF/VLF increases with the increase of effective radiation power, while the radiation efficiency increases first and then decreases;
- (2) the X-mode is better than the O-mode;
- (3) the radiation intensity of ELF/VLF decreases with the increase of pump wave frequency from 4MHz to 10MHz;
- (4) the ELF/VLF equivalent dipole moments increase with the rise of modulation frequency from 500Hz to 5KHz;
- (5) with the change of duty cycle from 10% to 90%, the dipole moments first increase and then decrease, and the optimal range of duty cycle is 40% to 70%;
- (6) with the increase of bandwidth, the dipole moments are unchanged;
- (7) the ELF/VLF dipole moments of square wave amplitude modulated heating ionosphere is unchanged before and after the chirp spread spectrum.

ACKNOWLEDGMENT

The data used in this study were obtained from the International Reference Ionosphere (IRI): <http://iri.gsfc.nasa.gov/>, Mass Spectrometer Incoherent Scatter Atmosphere (NPLMSISE-00): <http://ccmc.gsfc.nasa.gov/>. The author would like to thank the IRI and NPLMSISE-00 for the high-quality data and successful operation.

REFERENCES

- [1] M. B. Cohen, R. K. Said, and U. S. Inan, "Mitigation of 50-60 Hz power line interference in geophysical data," *Radio Sci.*, vol. 45, no. 6, pp. 1-12, Dec. 2010.
- [2] S. P. Kuo, "Ionospheric very low frequency transmitter," *Phys. Plasmas*, vol. 22, no. 2, p. 9073, 2015.
- [3] H. Rowe, "Extremely low frequency (ELF) communication to submarines," *IEEE Trans. Commun.*, vol. 22, no. 4, pp. 371-385, Apr. 1974.
- [4] J. W. Willis and J. R. Davis, "Radio frequency heating effects on electron density in the lower E region," *J. Geophys. Res. Atmos.*, vol. 78, no. 78, pp. 5710-5717, 1973.
- [5] G. G. Getmantsev, N. A. Zuikov, D. S. Kotik, L. F. Mironenko, N. A. Mitiakov, V. O. Rapoport, I. A. Sazonov, V. I. Trakhtengerts, and V. I. Eidman, "Combination frequencies in the interaction between high-power short-wave radiation and ionospheric plasma," *ZhPmR*, vol. 20, pp. 229-232, Aug. 1974.
- [6] R. Barr and P. Stubbe, "ELF radiation from the Tromsø 'super heater' facility," *Geophys. Res. Lett.*, vol. 18, no. 6, pp. 1035-1038, Jun. 1991.
- [7] M. B. Cohen, R. C. Moore, M. Golkowski, and N. G. Lehtinen, "ELF/VLF wave generation from the beating of two HF ionospheric heating sources," *J. Geophys. Res. Atmos.*, vol. 117, no. 12, pp. 1702-1711, 2012.
- [8] R. Moore, *ELF/VLF Wave Generation by Modulated HF Heating of the Auroral Electrojet*. Stanford, CA, USA: Stanford Univ., 2007.
- [9] K. Papadopoulos, C. L. Chang, P. Vitello, and A. Drobot, "On the efficiency of ionospheric ELF generation," *Radio Sci.*, vol. 25, no. 6, pp. 1311-1320, Nov. 1990.
- [10] M. B. Cohen, U. S. Inan, and M. A. Golkowski, "Geometric modulation: A more effective method of steerable ELF/VLF wave generation with continuous HF heating of the lower ionosphere," *Geophys. Res. Lett.*, vol. 35, no. 12, pp. 62-77, 2008.

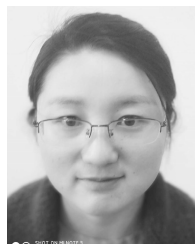
- [11] S. P. Kuo, M. C. Lee, P. Kossey, K. Groves, and J. Heckscher, "Stimulated thermal instability for ELF and VLF wave generation in the polar electrojet," *Geophys. Res. Lett.*, vol. 27, no. 1, pp. 85–88, 2000.
- [12] G. M. Milikh and K. Papadopoulos, "Enhanced ionospheric ELF/VLF generation efficiency by multiple timescale modulated heating," *Geophys. Res. Lett.*, vol. 34, no. 20, pp. 1–5, 2007.
- [13] D. Agrawal and R. C. Moore, "Dual-beam elf wave generation as a function of power, frequency, modulation waveform, and receiver location," *J. Geophys. Res. Atmos.*, vol. 117, no. 12, p. 12305, 2012.
- [14] R. Barr and P. Stubbe, "ELF and VLF wave generation by HF heating: A comparison of AM and CW techniques," *J. Atmos. Sol.-Terr. Phys.*, vol. 59, no. 18, pp. 2265–2279, Dec. 1997.
- [15] M. B. Cohen and M. Gołkowski, "100 days of ELF/VLF generation via HF heating with HAARP," *J. Geophys. Res., Space Phys.*, vol. 118, no. 10, pp. 6597–6607, Oct. 2013.
- [16] M. B. Cohen, U. S. Inan, M. Gołkowski, and M. J. McCarrick, "ELF/VLF wave generation via ionospheric HF heating: Experimental comparison of amplitude modulation, beam painting, and geometric modulation," *J. Geophys. Res., Space Phys.*, vol. 115, no. 2, pp. 1–10, Feb. 2010.
- [17] G. Jin, M. Spasojevic, M. B. Cohen, and U. S. Inan, "Utilizing nonlinear ELF generation in modulated ionospheric heating experiments for communications applications," *Radio Sci.*, vol. 48, no. 1, pp. 61–68, Jan. 2013.
- [18] H. O. Ramp and E. R. Wingrove, "Principles of pulse compression," *IRE Trans. Mil. Electron.*, vol. 5, no. 2, pp. 109–116, Apr. 1961.
- [19] R. Dixon, *Spread Spectrum Techniques*. New York, NY, USA: IEEE, 1976, pp. 1–14.
- [20] M. Winkley, "Chirp signals for communications," in *Proc. IEEE WESCON Conf.*, Jan. 1962, pp. 14–17.
- [21] Y.-R. Tsai and J.-F. Chang, "The feasibility of combating multipath interference by chirp spread spectrum techniques over Rayleigh and Rician fading channels," in *Proc. IEEE 3rd Int. Symp. Spread Spectr. Techn. Appl. (ISSSTA)*, Jul. 1994, pp. 282–286.
- [22] Y. Sarni, R. Sadoun, and A. Belouchrani, "On the application of chirp modulation in spread spectrum communication systems," in *Proc. 6th Int. Symp. Signal Process. Appl.*, vol. 2, Aug. 2001, pp. 501–504.
- [23] J. Villaseñor, A. Y. Wong, B. Song, J. Pau, M. McCarrick, and D. Sentman, "Comparison of ELF/VLF generation modes in the ionosphere by the HIPAS heater array," *Radio Sci.*, vol. 31, no. 1, pp. 211–226, Jan. 1996.
- [24] M. Gołkowski, M. B. Cohen, and R. C. Moore, "Modulation of auroral electrojet currents using dual modulated HF beams with ELF phase offset, a potential D-region ionospheric diagnostic," *J. Geophys. Res., Space Phys.*, vol. 118, no. 5, pp. 2350–2358, May 2013.
- [25] J. R. Wait and K. P. Spies, *Characteristics of the Earth-Ionosphere Waveguide for VLF Radio Waves*, vol. 13. US Department of Commerce, National Bureau of Standards, 1964.
- [26] N. R. Thomson, C. J. Rodger, and M. A. Clilverd, "Daytime d region parameters from long-path VLF phase and amplitude," *J. Geophys. Res., Space Phys.*, vol. 116, no. 11, pp. 1–12, 2011.
- [27] N. R. Thomson, M. A. Clilverd, and W. M. McRae, "Nighttime ionospheric D region parameters from VLF phase and amplitude," *J. Geophys. Res., Space Phys.*, vol. 112, no. 7, p. 39, 2007.
- [28] A. S. Maxworth, M. Gołkowski, M. B. Cohen, R. C. Moore, H. T. Chorsi, S. D. Gedney, and R. Jacobs, "Multistation observations of the azimuth, polarization, and frequency dependence of ELF/VLF waves generated by electrojet modulation," *Radio Sci.*, vol. 50, no. 10, pp. 1008–1026, Oct. 2015.
- [29] M. B. Cohen, M. Golkowski, N. G. Lehtinen, U. S. Inan, and M. J. McCarrick, "HF beam parameters in ELF/VLF wave generation via modulated heating of the ionosphere," *J. Geophys. Res., Space Phys.*, vol. 117, no. 5, pp. 1–10, May 2012.



KAIJIE ZHOU received the B.S. degree in electrical engineering and automation from the Hefei University of Technology, Hefei, China, in 2007, and the M.S. degree in electrical theory and new technology from Shandong University. He is currently pursuing the Ph.D. degree in signal and information processing with PLA Army Engineering University, Nanjing, China. His research interests include wireless communication and physical-layer security.



HUALI WANG (Member, IEEE) received the Ph.D. degree in electronic engineering from the University of Science and Technology, China, in 1997. He is currently a Professor with the Nanjing College of Communication Engineering, PLA Army Engineering University, Nanjing, China. His research interests include wireless communication and physical-layer security.



PEIPEI CAO received the M.S. degree in communication engineering from Shanghai Maritime University, Shanghai, China, in 2011. She is currently pursuing the Ph.D. degree with the Nanjing University of Science and Technology. Her research interests include weak signal detection and processing.